Journal of Marine Science and Technology
https://doi.org/10.1007/s00773-024-01036-w

ORIGINAL ARTICLE

Data augmentation methods of dynamic model identification for harbor maneuvers using feedforward neural network

Kouki Wakita[1] · **Yoshiki Miyauchi**[1] · **Youhei Akimoto**[2,3] · **Atsuo Maki**[1]

Received: 17 May 2023 / Accepted: 26 October 2024

Abstract
A dynamic model for an automatic berthing and unberthing controller has to estimate harbor maneuvers, which include berthing, unberthing, approaching maneuvers to berths, and entering and leaving the port. When the dynamic model is estimated by the system identification using feedforward neural networks, a large number of tests or trials are required to measure the various motions of harbor maneuvers. However, the amount of data that can be obtained is limited due to the high costs and time-consuming nature of full-scale ship trials. Therefore, this paper introduces data augmentation to improve the generalization performance of dynamic models identified from a limited dataset. This study used slicing and jittering as data augmentation methods and confirmed their effectiveness by numerical experiments using the free-running model tests. Results of numerical experiments demonstrated that slicing and jittering are effective data augmentation methods but could not improve generalization performance for extrapolation states of the original dataset.

Keywords Jittering · Slicing · Neural network · Maneuvering model

1 Introduction

There is a growing interest in the research and development of control algorithms and automatic navigation systems for maritime autonomous surface ships (MASS). Dynamic models can be used to design and tune control algorithms and provide a verification environment for automatic navigation systems. Therefore, dynamic models that can simulate maneuvering motions are beneficial for MASS.

One of the technical challenges in achieving MASS is the development of the automatic berthing and unberthing controller, which requires an appropriate dynamic model. To achieve berthing, the ship's speed needs to be significantly reduced before reaching the berth. In addition, various maneuvering motions such as turning tightly, astern, and crabbing may be required depending on the port and shape of the berth. In essence, a dynamic model for the automatic berthing and unberthing controller must be capable of estimating harbor maneuvers, which include various maneuvers like berthing and unberthing, approaching maneuvers to berths, and entering and leaving the port.

Moreover, when ships are controlled by algorithms like optimal control or reinforcement learning, maneuvers that do not exist in human operations may occur, and the dynamic model has to evaluate such maneuvers properly. Therefore, a dynamic model for the automatic berthing and unberthing controller is desirable to estimate all possible ship motions at low speeds.

Numerous studies have been conducted on the dynamic model for the ship maneuvering motion. In particular, many studies have focused on the modeling of the hydrodynamic force acting on the ship.

For instance, one of the dynamic models for the ship maneuvering motion is the Abkowitz model [1]. The Abkowitz model represents the hydrodynamic force by polynomials. These polynomials are obtained from a Taylor expansion about the uniform linear forward motion condition. The model is simple to derive and can be added with nonlinear terms, which enables it to represent a wider range of ship maneuvering behaviors.

✉ Kouki Wakita
kouki_wakita@naoe.eng.osaka-u.ac.jp

[1] Osaka University, 2-1 Yamadaoka, Suita, Osaka, Japan

[2] Faculty of Engineering, Information and Systems, University of Tsukuba, 1-1-1 Tennodai, Tsukuba, Ibaraki 305-8573, Japan

[3] RIKEN Center for Advanced Intelligence Project, 1-4-1 nihonbashi, Chuo-ku, Tokyo 103-0027, Japan

Published online: 20 November 2024

Besides, the MMG model, which was proposed by a research group of the Japan Towing Tank Conference [2], is also one of the dynamic models applicable for simulating ship motions. The MMG model is a modular-type mathematical model consisting of submodels, which express the hydrodynamic force induced by the hull, propeller, rudder, and other actuators. Thus, the MMG model only requires modification of the relevant submodels even if partial design changes occur, such as changes to the rudder.

The standard MMG model [3] and classical Abkowitz model [1] are primarily focused on ship maneuvering in which the ship's forward speed is sufficiently large and steady. These models are not supposed to predict harbor maneuvers. However, several studies have been conducted on the modification of the MMG model for low-speed maneuvering [4–8]. Miyauchi et al. expanded the Abkowitz model for harbor maneuver [9] and then proposed an automatic derivation method of a hybrid model combining the MMG and Abkowitz models for harbor maneuvering motions [10]. Those studies have enabled the MMG and Abkowitz models to represent a greater variety of maneuvering behaviors.

Parameters included in dynamic models are often estimated by captive model tests [3, 11–13] and empirical formulas [8, 14–18]. For example, added mass and added moment of inertia can be estimated from Motora's chart [14], and the coefficients of hydrodynamic force on the hull can be estimated from Inoue's formula [16], Kijima's formula [17], and Yoshimura's formula [8]. The rudder lift gradient coefficient can be estimated using Fujii's formula [15] and the wind pressure coefficients using Fujiwara's regression formulae [19]. Although these empirical formulas can estimate most of the coefficients of the standard maneuvering model, it is not always possible to estimate the special coefficients of the low-speed maneuvering model from charts and formulas. Captive model tests can provide much information to estimate parameters by measuring the forces acting on the ship, and planar motion mechanism (PMM) tests [11] and the circular motion tests (CMT) [12] are often conducted. However, captive model tests require special test facilities, and although the number of experiments may be reduced by using empirical formulas and past experimental results, the experiments require a significant amount of time and effort.

System identification (SI) is often used as an alternative method. SI techniques require time series data of kinematic variables and control inputs measured during free-running model tests or full-scale ship tests and essentially do not require force and moment measurements.

SI is often divided into two categories: parametric SI and non-parametric SI. Parametric SI is an SI method based on a priori information about the system of interest, and in many cases, such a priori information is incorporated into the dynamic model.

Many studies have been conducted on Parametric SI for the ship's maneuver, and various identification methods have been proposed [1, 20–25]. Åström and Källström [20, 26] applied the maximum likelihood method to determine the ship steering dynamics from measurements of a freighter and a tanker. Abkowitz [1] proposed the identification method for the hydrodynamic coefficients and tidal current state based on the extended Kalman filter. Yoon and Rhee [21] used ridge regression to estimate the hydrodynamic coefficient of the polynomial model from sea trial data smoothed by a modified Bryson-Frazier smoother. Sutulo et al. [23] proposed an identification method based on the classic genetic algorithm used to minimize the distance between the observed state history and time series data recovered by maneuvering simulation. Miyauch et al. [24] applied the covariance matrix adaptation evolution strategy to explore the system parameters of the MMG model using the free-running model tests.

In non-parametric SI, the input–output relationship of a dynamic model is modeled from data without prior information about the target system. Well-known methods are artificial neural networks (ANNs) [25, 27–31] and kernel methods such as support vector regression (SVR) [32, 33] and Gaussian processes (GP) [34, 35]. Although no prior physical or hydrodynamic knowledge is used, the method is applicable regardless of the actuator configuration and has the ability to capture the nonlinear characteristics of the target system.

ANN is a multi-input, multi-output model that has high approximation capabilities [36, 37]. Their effectiveness in estimating maneuvering models has been demonstrated in prior research. For instance, Moreira et al. [27, 28] proposed a maneuvering simulation model using an ANN model, validated through the use of simulation data from the Mariner hull and full-scale data from a catamaran. Rajesh et al. [29] utilized ANN to represent the nonlinear terms within the 3DOF maneuvering model for large tankers. Oskin et al. [30] used an ANN model that takes past and current state variables as inputs to identify a model of a ship's course movement. Zhang et al. [31] identified the nonlinear hydrodynamic model of ship maneuvering motion using an ANN with Chebyshev orthogonal basis functions.

SI requires an appropriate dataset in accordance with the purpose of the dynamic model. A dataset that covers the operational range of a harbor maneuver should be used to identify a dynamic model for the automatic berthing and unberthing controller.

Most SI studies for a ship maneuvering model use the data measured during zigzag and turning maneuvers of the full-scale trials or free-running model tests. However, zigzag and turning tests are not suitable for estimating the dynamic model for harbor maneuvers since they cannot measure harbor maneuvers, such as astern and crabbing motions.

Several previous studies [10, 24, 25] used the dataset measured in random maneuvers. Here, random maneuvers are maneuvers in which control inputs are manually selected to measure the various values of state variables and control inputs that can occur.

Identifying a dynamic model for harbor maneuvers requires conducting a large number of tests or trials to measure various motions. However, conducting numerous full-scale ship trials is impractical due to the high cost involved. Therefore, a method for identifying a dynamic model with a limited amount of data is required. One of the options to achieve the high generalization performance of dynamic models is to apply data augmentation, which generates synthetic data.

Many studies have been conducted on data augmentation methods that can be applied to time series data [38, 39]. However, to the best of our knowledge, no studies have been conducted on applying data augmentation methods to dynamic model identification of ship maneuvering motions.

Furthermore, a problem of data augmentation is that not all data augmentation techniques necessarily improve the generalization performance of the ship's dynamic model.

In fact, many generation methods of synthetic data distort the meaning of the original data. For example, window wrapping [40–42], which is one of the time wrapping methods, generates synthetic data by compressing or stretching time series data. This should not be applied to this problem since the time derivative of the state variable predicted by the dynamic model may be changed significantly. These data augmentation methods may cause the deterioration of the generalization performance by generating data whose characteristics are different from that of the original data.

This study aims to improve the generalization performance of the dynamic model for harbor maneuvers by introducing data augmentation. For this purpose, this study demonstrates effective data augmentation methods and their effectiveness. In this paper, slicing [40, 43] and jittering [41, 44, 45] are introduced as the data augmentation methods. These data augmentation methods are applied to the identification problem of the dynamic model using ANN. Numerical experiments are conducted to demonstrate the effectiveness of the data augmentation methods, utilizing the dataset measured in free-running model tests. The free-running model test included measurements of random maneuvers and manual berthing maneuvers with an imaginary berth.

The contents of this paper overlap the previous literature [46], but presents the results more extensively, with some revisions.

The remainder of this paper is organized as follows: Sect. 2 defines the identification methods of the dynamic model; Sect. 3 describes data augmentation methods; Sect. 4 shows numerical experiments to show the effectiveness of the data augmentation methods; Sect. 5 discuss the numerical experiments and future works; finally, Sect. 6 concludes this paper.

2 Identification methods

In this section, we describe the identification method of the dynamic model using time series data obtained from full-scale ship trials or free-running model tests. In this study, the metric of the prediction error of the dynamic model was defined, and the identification method was formulated as a minimization problem of the prediction error. The parameters of the dynamic model are identified by finding the optimal parameter minimizing the prediction error metric. This method is partly based on the previous study [25]. First, The coordinate systems and state variables were defined in Sect. 2.1. Next, the used mathematical model are described in Sect. 2.2. Then, Sect. 2.3 describe the identification method.

2.1 Coordinate systems

The earth-fixed coordinate system $\mathrm{O}-x_0y_0$ and a ship-fixed coordinate system $\mathrm{O}-xy$ are defined as Fig. 1. Note that the origin of the coordinate system $\mathrm{O}-xy$ is fixed at the midship. Then, the subject ship of this study is the model ship equipped with a single-propeller, VecTwin rudder, and a bow thruster, and is shown in Fig. 2. The port and starboard side rudder angle is defined as δ_p and δ_s, respectively. The propeller revolution number is n_p. These actuator states are defined as $\boldsymbol{u} \equiv \left(\delta_\mathrm{p}, \delta_\mathrm{s}, n_\mathrm{p}\right)^\mathsf{T} \in \mathbb{R}^3$. Note that this study used a bow thruster revolution number of zero.

The ship's position is represented by x_0, y_0, and the heading angle from the x_0 axis is ψ. The surge, sway (at midship), and yaw angle velocity are denoted as u, v_m, and

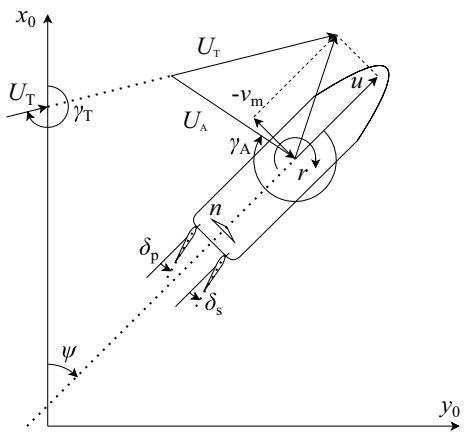

Fig. 1 Coordinate systems

Fig. 2 Subject model ship at the experimental pond

r, respectively. These ship state variables are defined as $\boldsymbol{x} \equiv \left(x_0, u, y_0, v_\mathrm{m}, \psi, r\right)^\mathsf{T} \in \mathbb{R}^6$. For the convenience of explanation, the ship position and heading angle are defined as $\boldsymbol{\eta} \equiv \left(x_0, y_0, \psi\right)^\mathsf{T} \in \mathbb{R}^3$ and the surge, sway, and yaw angle velocity are defined as $\boldsymbol{\nu} \equiv \left(u, v_\mathrm{m}, r\right)^\mathsf{T} \in \mathbb{R}^3$. The true wind speed and wind direction are defined as U_T and γ_T, respectively. The apparent wind speed and direction are U_A and γ_A, respectively. The apparent wind states are defined as $\boldsymbol{\omega} = (U_\mathrm{A},\ \gamma_\mathrm{A})^\mathsf{T} \in \mathbb{R}^2$. This study assumes that the wind speed and direction are uniform in space and depend on the physical time.

2.2 Neural network-based dynamic model

The effect of waves is not considered in this study and currents are ignored for simplicity since this study focuses on harbor maneuvers. Therefore, the dynamics of ship motions are assumed to be expressed by the nonlinear ordinary differential equation as follows:

$$\dot{\boldsymbol{\nu}}(t) = \boldsymbol{F}(\boldsymbol{\nu}(t), \boldsymbol{u}(t), \boldsymbol{\omega}(t)) \ . \tag{1}$$

Here, $\dot{\boldsymbol{\nu}}$ donates the time derivative of $\boldsymbol{\nu}$.

The nonlinear function $\boldsymbol{F}$ is modeled by the NN model.

NN is a mathematical model inspired by the human brain. This model is known as the model that has high approximation capabilities [36, 37]. In this study, an NN model consisting only of fully connected layers, called feedforward NN (FNN), is used. Let input and output variables denotes $\boldsymbol{s}$ and $\boldsymbol{y}$, respectively, FNN with L hidden layers are defined as follows:

Table 1 The network architecture of the dynamic model

$L = 4$	Weight $\boldsymbol{W}_l$	Bias $\boldsymbol{b}_l$	Activation function $\boldsymbol{g}_l$
$l = 1$	$\mathbb{R}^{256\times8}$	$\mathbb{R}^{256}$	Hyperbolic tangent
$l = 2, 3, 4$	$\mathbb{R}^{256\times256}$	$\mathbb{R}^{256}$	Hyperbolic tangent
$l = 5$	$\mathbb{R}^{3\times256}$	$\mathbb{R}^{3}$	None

$$\begin{cases} \boldsymbol{z}_1 = \boldsymbol{g}_1\left(\boldsymbol{W}_1\boldsymbol{s} + \boldsymbol{b}_1\right) \\ \quad \vdots \\ \boldsymbol{z}_L = \boldsymbol{g}_L\left(\boldsymbol{W}_L\boldsymbol{z}_{L-1} + \boldsymbol{b}_L\right) \\ \boldsymbol{y} = \boldsymbol{g}_{L+1}\left(\boldsymbol{W}_{L+1}\boldsymbol{z}_L + \boldsymbol{b}_{L+1}\right) \ , \end{cases} \tag{2}$$

where $\boldsymbol{z}_l$ denote variables of l-th hidden layer, and $\boldsymbol{g}_l$, $\boldsymbol{W}_l$, and $\boldsymbol{b}_l$ denote the activation function, weight matrix, and bias vector for the transformation to the l-th hidden layer, respectively. The dimensions of parameters and the activation functions for each layer are listed in Table 1.

Scale differences in NN inputs are likely to make the optimization problem challenging. Therefore, the NN inputs were standardized using the mean and standard deviation of the training data. The standardized variables of $\boldsymbol{\nu}, \boldsymbol{u}, \boldsymbol{\omega}$ are defined as $\bar{\boldsymbol{\nu}}, \bar{\boldsymbol{u}}, \bar{\boldsymbol{\omega}}$, respectively. The j-th components of $\bar{\boldsymbol{\nu}}, \bar{\boldsymbol{u}}, \bar{\boldsymbol{\omega}}$ are represented as follows:

$$\begin{aligned} \bar{\nu}_j &= \left(\nu_j - \mu^{(\mathrm{train})}_{\nu,j}\right) / \left(\sigma^{(\mathrm{train})}_{\nu,j}\right) \ , \\ \bar{u}_j &= \left(u_j - \mu^{(\mathrm{train})}_{u,j}\right) / \left(\sigma^{(\mathrm{train})}_{u,j}\right) \ , \\ \bar{\omega}_j &= \left(\omega_j - \mu^{(\mathrm{train})}_{\omega,j}\right) / \left(\sigma^{(\mathrm{train})}_{\omega,j}\right) \ , \end{aligned} \tag{3}$$

where $\mu^{(\mathrm{train})}_{\nu,j}$, $\mu^{(\mathrm{train})}_{u,j}$, and $\mu^{(\mathrm{train})}_{\omega,j}$ denotes the j-th components of the mean of $\boldsymbol{\nu}$, $\boldsymbol{u}$, and $\boldsymbol{\omega}$, respectively, and $\sigma^{(\mathrm{train})}_{\nu,j}$, $\sigma^{(\mathrm{train})}_{u,j}$, $\sigma^{(\mathrm{train})}_{\omega,j}$ denotes the j-th components of the standard deviation of $\boldsymbol{\nu}$, $\boldsymbol{u}$, and $\boldsymbol{\omega}$. Then, the NN inputs are defined as $\boldsymbol{s} = \left(\bar{\boldsymbol{\nu}}^\mathsf{T}, \bar{\boldsymbol{u}}^\mathsf{T}, \bar{\boldsymbol{\omega}}^\mathsf{T}\right)^\mathsf{T} \in \mathbb{R}^8$

Furthermore, the NN outputs are also assumed to be standardized variables. Thus, the j-th components of $\dot{\boldsymbol{\nu}}$ are calculated as follows:

$$\dot{\nu}_j = \sigma^{(\mathrm{train})}_{\mathrm{acc},j} \cdot y_j + \mu^{(\mathrm{train})}_{\mathrm{acc},j} \ , \tag{4}$$

where y_j denotes the j-th components of $\boldsymbol{y}$, and $\mu^{(\mathrm{train})}_{\mathrm{acc},j}$ and $\sigma^{(\mathrm{train})}_{\mathrm{acc},j}$ denotes the mean and standard deviation of the j-th components of $\dot{\boldsymbol{\nu}}$. These statistical values are computed based on the training dataset. Note that $\dot{\boldsymbol{\nu}}$ was not measured.

Instead, $\dot{\boldsymbol{\nu}}$ was calculated using numerical differentiation to derive these statistical values.

In summary, the dynamic model is represented by the composite function of Eqs. 2–4.

Besides, the time derivative of the ship position and heading angle $\dot{\boldsymbol{\eta}}$ are expressed as follows:

$$\dot{\boldsymbol{\eta}} = \begin{bmatrix} \cos\psi & -\sin\psi & 0 \\ \sin\psi & \cos\psi & 0 \\ 0 & 0 & 1 \end{bmatrix} \boldsymbol{\nu} \ , \tag{5}$$

where $\dot{\boldsymbol{\eta}}$ donates the time derivative of $\boldsymbol{\eta}$.

For convenience, the dynamic model and Eq. 5 are collectively denoted as follows:

$$\dot{\boldsymbol{x}}(t) = \boldsymbol{f}(\boldsymbol{x}(t), \boldsymbol{u}(t), \boldsymbol{\omega}(t); \boldsymbol{\theta}) \ , \tag{6}$$

where $\boldsymbol{\theta}$ denotes the parameters of the dynamic model, including all weight matrices and bias vectors.

2.3 Optimization problem

The identification method used in this study was formulated as a minimization problem of the prediction error metric of the dynamic model. The prediction error was calculated by comparing the measured state variables and the state variable simulated by the dynamic model. The method was described in the remainder of this subsection.

Let us assume that the time series of ship state variables $\boldsymbol{x}$ and actuator state variables $\boldsymbol{u}$, apparent wind state variables $\boldsymbol{\omega}$ were given, and N denote the number of time series. This dataset is defined as follows:

$$\mathscr{D} \equiv \left\{ \left(\boldsymbol{x}_n(t), \boldsymbol{u}_n(t), \boldsymbol{\omega}_n(t) \mid t \in [t_{0,n}, t_{1,n}] \right) \right\}_{n=1,2,\ldots,N} . \tag{7}$$

where $t_{0,n}$ and $t_{1,n}$ denotes the start and end time of the time series data, and the subscript n indicates that it is the n-th time series data.

The ship state variables can be simulated with the use of a dynamic model and the given dataset. The simulated ship state variables $\boldsymbol{x}_n^{\mathrm{sim}}$ is expressed as follows:

$$\begin{aligned} \boldsymbol{x}_n^{\mathrm{sim}}(t;\boldsymbol{\theta}) &= \boldsymbol{x}_n(t_{0,n}) \\ &\quad + \int_{t_{0,n}}^{t} \boldsymbol{f}\left(\boldsymbol{x}_n^{\mathrm{sim}}(\tau;\boldsymbol{\theta}), \boldsymbol{u}_n(\tau), \boldsymbol{\omega}_n(\tau); \boldsymbol{\theta} \right) \mathrm{d}\tau \\ &\qquad \text{for} \quad n = 1, 2, \ldots, N \ . \end{aligned} \tag{8}$$

The prediction error of the dynamic model is defined by comparing these simulated ship state variables $\boldsymbol{x}_n^{\mathrm{sim}}$ with that of the dataset $\boldsymbol{x}_n$. The evaluation function of the prediction error is defined as follows:

$$\mathscr{L}(\boldsymbol{\theta}; \mathscr{D}) = \frac{1}{N} \sum_{n=1}^{N} \left\{ \int_{t_{0,n}}^{t_{1,n}} d\left(\boldsymbol{x}_n^{\mathrm{sim}}(t;\boldsymbol{\theta}), \boldsymbol{x}_n(t) \right) \mathrm{d}t \right\} \ , \tag{9}$$

where, $d\left(\boldsymbol{x}^{\mathrm{sim}}, \boldsymbol{x}\right)$ is a function that returns the error between $\boldsymbol{x}^{\mathrm{sim}}$ and $\boldsymbol{x}$ as a scalar value, and defined as follows:

$$d\left(\boldsymbol{x}^{\mathrm{sim}}, \boldsymbol{x}\right) = \left\| \boldsymbol{w} \cdot \left(\boldsymbol{x}^{\mathrm{sim}} - \boldsymbol{x} \right) \right\|^2 \ . \tag{10}$$

Here, $\boldsymbol{w} \in \mathbb{R}^6$ is a weight vector. This weight vector was introduced to compensate for the scale differences of state variables.

Although the model parameters can be identified by minimizing the prediction error defined in Eq. 9, a regularization term was added to the optimization target to avoid overfitting. Thus, the model parameters identified in the dataset are represented as follows:

$$\boldsymbol{\theta}_{\mathrm{opt}} = \mathrm{argmin} \left\{ \mathscr{L}(\boldsymbol{\theta}; \mathscr{D}) + \lambda \|\boldsymbol{\theta}\|^2 \right\} \ , \tag{11}$$

where λ is the regularization parameter.

Although the time series data of Eq. 7 are defined as continuous time values, the actual measured time series data are given as discrete time values. Thus, the dataset obtained from the full-scale ship trials or free-running model tests is expressed as follows:

$$\mathscr{D} \equiv \left\{ \left(\boldsymbol{x}_n(t_i), \boldsymbol{u}_n(t_i), \boldsymbol{\omega}_n(t_i) \right)_{i=0,1,\ldots,I_n-1} \right\}_{n=1,2,\ldots,N} . \tag{12}$$

Here, the t_i represents the physical time of the i-th time step, and I_n denotes the number of time steps in the n-th time series data.

It is hard to calculate Eqs. 9 and 8 analytically. Therefore, this study calculated the time integration of Eq. 9 by trapezoidal approximation as follows:

$$\mathscr{L}(\boldsymbol{\theta}; \mathscr{D}) = \frac{1}{N} \sum_{n=1}^{N} \left\{ \sum_{i=0}^{I_n-2} \frac{d_{n,i+1} + d_{n,i}}{2} \Delta t_i \right\} \ , \tag{13}$$

where, $d_{n,i} = d\left(\boldsymbol{x}_n^{\mathrm{sim}}(t_i;\boldsymbol{\theta}), \boldsymbol{x}_n(t_i) \right)$, $\Delta t_i = t_{i+1} - t_i$.

The simulated ship state variables $\boldsymbol{x}_n^{\mathrm{sim}}$ were obtained by using the Euler method, as follows:

$$\begin{aligned} \boldsymbol{x}_n^{\mathrm{sim}}(t_i;\boldsymbol{\theta}) &= \boldsymbol{x}_n(t_0) \\ &\quad + \sum_{k=0}^{i-1} \Delta t_k \cdot \boldsymbol{f}\left(\boldsymbol{x}_n^{\mathrm{sim}}(t_k;\boldsymbol{\theta}), \boldsymbol{u}_n(t_k), \boldsymbol{\omega}_n(t_k); \boldsymbol{\theta} \right) \\ &\qquad \text{for} \quad n = 1, 2, \ldots, N \ . \end{aligned} \tag{14}$$

Equations 13 and 14 can be easily calculated numerically.

The parameters $\boldsymbol{\theta}$ are optimized by a gradient descent-based optimization method, Adam [47]. Gradients with respect to the parameters were computed using the back-propagation method, and PyTorch, an open-source Python

library for machine learning, was used for the implementation. In optimizing the NN model, the training dataset was randomly split into three subsets, and we computed the gradients and updated parameters for each subset. The number of cycles that pass through a training dataset is called an epoch.

3 Data augmentation methods

This section describes the data augmentation methods applied to the identification problem described in Sect. 2.

Data augmentation generates synthetic data by transforming the original dataset. In this study, we focus on magnitude and time domain transformation-based data augmentation methods introduced in the previous study [39]. These methods are performed by transforming values or the time axis of time series data and include jittering, rotation, scaling, magnitude warping, slicing, permutation, and time warping. However, not all of these methods can be applied to the identification problem of Sect. 2. For example, the window warping method distorts the meaning of the data because the time derivative of the state variables (the acceleration) is changed significantly.

Among these methods, slicing [40, 43] and jittering [41, 44, 45] are expected to be applicable. Slicing generates synthetic data by extracting slices from the original time series. Slicing does not alter the meaning of the original data, as it does not affect the time derivative. On the other hand, jittering generates synthetic data by adding noise to the time series data. Jittering can generate data that resembles a different realization of sensor data when noise, whose magnitude is close to the observation accuracy, is used. Jittering also does not significantly distort the meaning of the original data if the appropriate noise is used. Therefore, this study employs slicing and jittering.

In this paper, the dataset without data augmentation is denoted as the reference dataset. The reference dataset is defined in Sect. 3.1, and the augmented dataset by Jittering and/or slicing is described in Sect. 3.3 to 3.4.

3.1 Definition of the reference dataset

The reference dataset without data augmentation is described here. The measured time series data do not necessarily have constant time steps. In other words, I_n in Eq. 12 is not necessarily constant for n. In this case, the computation of Eq. 14 requires a lot of time when the time step I_n is large. Therefore, the time-series data are divided by a certain number of time steps, and the divided time-series dataset is defined as a reference dataset.

The n-th time series data are divided by a constant number of time steps I ($< I_n$). The k-th time series data divided from the n-th time series data are expressed as follows:

$$\mathscr{D}_{n,k}^{(\mathrm{ref})} \equiv \left(\boldsymbol{x}_n\left(t_{kI+i}\right), \boldsymbol{u}_n\left(t_{kI+i}\right), \boldsymbol{\omega}_n\left(t_{kI+i}\right)\right)_{i=0,\ldots,I-1} . \tag{15}$$

Hence, the reference dataset can be obtained by dividing N time series data, and is represented as follows:

$$\mathscr{D}^{(\mathrm{ref})} \equiv \left\{ \left\{ \mathscr{D}_{n,k}^{(\mathrm{ref})} \right\}_{k=0,1,\ldots,K_n-1} \right\}_{n=1,2,\ldots,N} , \tag{16}$$

Here, K_n denotes the number of divisions and is determined as follows:

$$K_n = \left\lfloor \frac{I_n}{I} \right\rfloor , \tag{17}$$

where $\lfloor \cdot \rfloor$ denotes the floor function.

3.2 Data augmentation by slicing

Slicing generates synthetic data by extracting the data with a certain time step from the original time-series data. The extracted data are selected randomly [40] or by sliding the start time step [43]. This study used the latter method.

Slicing allows for the generation of a greater number of time series patterns by extracting multiple time-series data segments with overlap from a time series. The difference between slicing and the method described in Sect. 3.1 is illustrated in Fig. 3.

In the identification method described in Sect. 2, the estimation accuracy of the simulated ship state is dependent on the accuracy of the initial ship state $\boldsymbol{x}_n\left(t_0\right)$. Therefore, the application of slicing is expected to reduce the impact of observation errors contained in specific initial values.

In this paper, the time step of the extracted time series data is equivalent to I, and the start time step is defined as φ. Then, the extracted time series data are expressed as follows:

$$\mathscr{D}_{n,\varphi}^{(\mathrm{sli})} \equiv \left(\boldsymbol{x}_n\left(t_{\varphi+i}\right), \boldsymbol{u}_n\left(t_{\varphi+i}\right), \boldsymbol{\omega}_n\left(t_{\varphi+i}\right)\right)_{i=0,\ldots,I-1} . \tag{18}$$

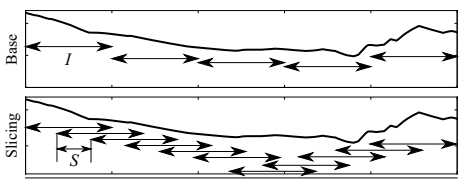

Fig. 3 Illustration of the reference and slicing dataset

Here, $0 \leq \varphi \leq I_n - I$ must be satisfied. In this study, we extract data by sliding φ at a step interval S. Thus, the dataset augmented by slicing is defined as follows:

$$\mathscr{D}^{(\mathrm{sli})} \equiv \left\{ \left\{ \mathscr{D}^{(\mathrm{sli})}_{n,\varphi} \right\}_{\varphi=0,S,\ldots,\left\lfloor \frac{I_n-I}{S} \right\rfloor S} \right\}_{n=1,2,\ldots,N}. \tag{19}$$

3.3 Data augmentation by jittering

Jittering generates synthetic data by adding noise to the time series data. In NNs, it is well known that adding noise to model inputs prevents overfitting and improves generalization performance [44]. In addition, jittering could be applied to sensor data [41, 45], since this method assumes that time-series data contain noise.

Normal noise independent in time and space is added to the ship state variables, and not added to the actuator and wind state variables. The m-th normal noise vector added to the ship state variables $\boldsymbol{x}_n(t_i)$ is defined as $\boldsymbol{\epsilon}_{n,m}(t_i) \sim \mathcal{N}(\mathbf{0}, \boldsymbol{\Sigma}_{\boldsymbol{x}})$, where $\boldsymbol{\Sigma}_{\boldsymbol{x}}$ denotes the covariance matrix of the normal noise. The time series data to which noise is added is represented as follows:

$$\mathscr{D}^{(\mathrm{jit})}_{n,k,m} \equiv \left(\boldsymbol{x}_n(t_{kI+i}) + \boldsymbol{\epsilon}_{n,m}(t_{kI+i}), \boldsymbol{u}_n(t_{kI+i}), \boldsymbol{\omega}_n(t_{kI+i})\right)_{i=0,\ldots,I-1}. \tag{20}$$

Thus, the dataset augmented by a factor of M by jittering is represented as follows:

$$\mathscr{D}^{(\mathrm{jit})} \equiv \left\{ \left\{ \mathscr{D}^{(\mathrm{jit})}_{n,k,m} \right\}_{k=0,1,\ldots,K_n-1} \right\}_{n=1,2,\ldots,N,m=1,2,\ldots,M}. \tag{21}$$

Jittering can increase the amount of data in proportion to the number of noises it generates. However, unnecessarily large noise deteriorates estimation accuracy. Therefore, the covariance matrix $\boldsymbol{\Sigma}_{\boldsymbol{x}}$ of added noise was determined according to the observation accuracy of the measurement equipment.

3.4 Data augmentation by slicing and jittering

The data augmentation method that uses slicing and jittering simultaneously is not so difficult to accomplish. The synthetic data can be generated by adding noise to the time series data of Eq. 18. The generated time series data are expressed as follows:

$$\mathscr{D}^{(\mathrm{sli\times jit})}_{n,\varphi,m} \equiv \left(\boldsymbol{x}_n(t_{\varphi+i}) + \boldsymbol{\epsilon}_{n,m}(t_{\varphi+i}), \boldsymbol{u}_n(t_{\varphi+i}), \boldsymbol{\omega}_n(t_{\varphi+i})\right)_{i=0,\ldots,I-1}. \tag{22}$$

Thus, the dataset augmented by slicing and Jittering is defined as follows:

$$\mathscr{D}^{(\mathrm{sli\times jit})} \equiv \left\{ \left\{ \mathscr{D}^{(\mathrm{sli\times jit})}_{n,\varphi,m} \right\}_{\varphi=0,S,\ldots,\left\lfloor \frac{I_n-I}{S} \right\rfloor S} \right\}_{n=1,2,\ldots,N,m=1,2,\ldots,M}. \tag{23}$$

4 Numerical experiments

One of the purposes of this paper is to demonstrate the effectiveness of the data augmentation methods described in Sect. 3. Numerical experiments were conducted using datasets obtained from free-running model tests. In this section, the numerical experiments are described and the results are presented. Section 4.1 describes the prepared dataset, Sect. 4.2 describes the optimization method and result, and Sect. 4.3 shows the prediction results of the identified dynamic model.

4.1 Dataset

The free-running model tests were conducted at Inukai Pond, which is an experimental pond at Osaka University, and the time series data of the ship state variables $\boldsymbol{x}$, actuator state variables $\boldsymbol{u}$, and relative wind state variables $\boldsymbol{\omega}$ were measured. The upper and lower limits of the actuator state variables are presented in Table 2. The configuration of the observation equipment of the model ship was the same as in the previous study [10]. The x_0 and y_0 were calculated by transforming the measured position by Global Navigation Satellite System (GNSS) to the midship position. The heading angle ψ and yaw angle velocity r were measured by Fiber Optical Gyro (FOG). u and v_{m} were calculated from the speed over ground, the course over ground, and the heading angle measured by GNSS and FOG, respectively. The apparent wind speed U_{A} and direction γ_{A} were measured by an ultrasonic anemometer. Although the measurement frequency was 10 Hz, the data used for the identification were downsampled to 1 Hz.

In free-running model tests, random maneuvers and manual berthing maneuvers with an imaginary berth were

Table 2 Limit of control inputs

Variable	Maximum and minimum
n_{P} (rps)	[0, 12.5]
δ_{s} (deg.)	[−35, 105]
δ_{p} (deg.)	[−105, 35]

Table 3 Trajectory data collected by free-running model tests

Trajectory no.	Duration	Maneuver
No. 1	500.5 (s)	Random
No. 2	1801.8 (s)	Random
No. 3	500.5 (s)	Random
No. 4	1801.8 (s)	Random
No. 5	1201.2 (s)	Random
No. 6	1201.2 (s)	Random
No. 7	100.0 (s)	Berthing
No. 8	100.0 (s)	Berthing

The sampling frequency is 1 Hz

Table 4 Prepared dataset

Dataset name	Trajectory no.	Augmentation methods
$\mathscr{D}^{(\mathrm{ref})}$	No. 1 and 2	Sect. 3.1 ($I = 100$)
$\mathscr{D}^{(\mathrm{sli2})}$	No. 1 and 2	Sect. 3.2 ($I = 100, S = 50$)
$\mathscr{D}^{(\mathrm{sli10})}$	No. 1 and 2	Sect. 3.2 ($I = 100, S = 10$)
$\mathscr{D}^{(\mathrm{jit2})}$	No. 1 and 2	Sect. 3.3 ($I = 100, M = 2$)
$\mathscr{D}^{(\mathrm{jit10})}$	No. 1 and 2	Sect. 3.3 ($I = 100, M = 10$)
$\mathscr{D}^{(\mathrm{sli2\times jit2})}$	No. 1 and 2	Sect. 3.4 ($I = 100, S = 50, M = 2$)
$\mathscr{D}^{(\mathrm{sli10\times jit10})}$	No. 1 and 2	Sect. 3.4 ($I = 100, S = 10, M = 10$)
$\mathscr{D}^{(\mathrm{d\text{-}ref})}$	No. 1, 2, 3 and 4	Sect. 3.1 ($I = 100$)
$\mathscr{D}^{(\mathrm{validation})}$	No. 5	Sect. 3.1 ($I = 100$)
$\mathscr{D}^{(\mathrm{test\text{-}R})}$	No. 6	Sect. 3.1 ($I = 100$)
$\mathscr{D}^{(\mathrm{test\text{-}B})}$	No. 7 and 8	Sect. 3.1 ($I = 100$)

Eight different training datasets are prepared

conducted. This test has been previously employed in a previous study [24, 25]. In random maneuvers, control inputs are selected randomly by the human operator to collect datasets including various ship and actuator states. In this study, the operator handled the model ship with the aim of measuring widely distributed data, including motions with large drift angles in low-speed conditions, such as those encountered in harbor maneuvers. In addition, data on berthing maneuvers were measured for the test. The obtained trajectory data and their measurement times are shown in Table 3.

Trajectories No. 1 to No. 4 were used as training data, trajectory No. 5 as validation data, trajectory No. 6 as test data of random maneuvers, and trajectories No. 7 and 8 as test data of berthing maneuvers. We prepared eight different training datasets to show the effectiveness of the data augmentation methods. The prepared datasets and their augmentation methods are listed in Table 4. $\mathscr{D}^{(\mathrm{ref})}$ is a reference dataset without data augmentation. $\mathscr{D}^{(\mathrm{sli2})}$ and $\mathscr{D}^{(\mathrm{jit2})}$ are datasets that have been augmented to twice the amount of data by each data augmentation method, and

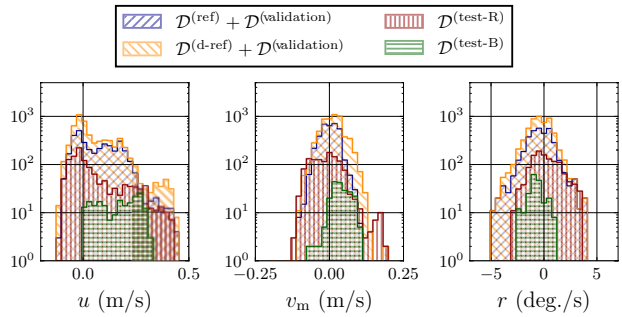

Fig. 4 Histograms of ship state variables. Note that the vertical axes, which show the frequency, are scaled logarithmically

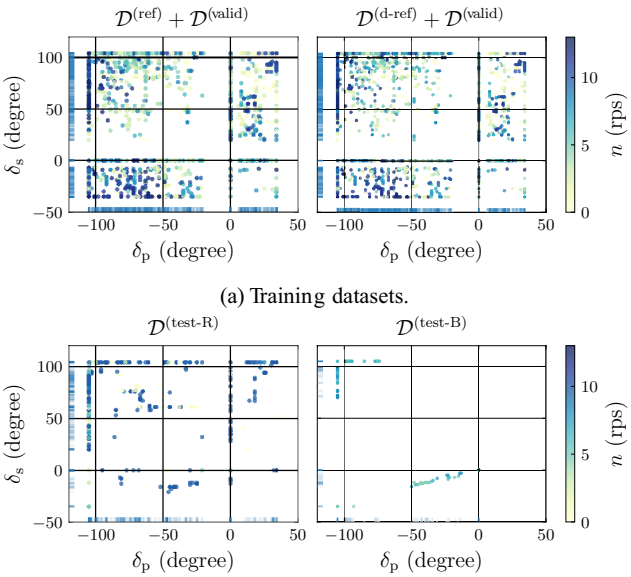

(a) Training datasets.

(b) Validation and test datasets.

Fig. 5 Scatter plots of δ_p, δ_s. The color bar shows the propeller revolution number n

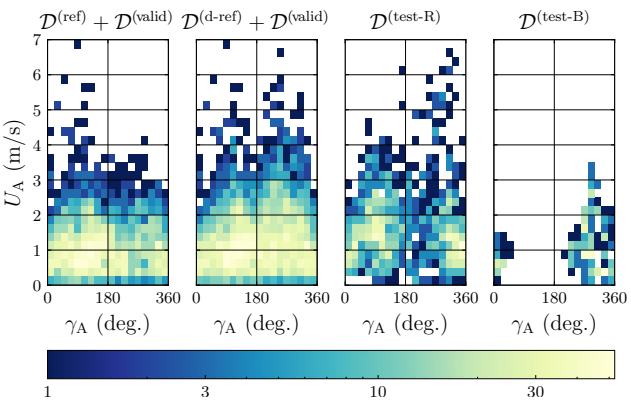

Fig. 6 2D histograms of apparent wind speed and direction. The bin width of apparent wind speed is 0.25 m/s, and that of apparent wind direction is 20 degrees. The color bar shows the frequency with a logarithmic scale

$\mathscr{D}^{(\text{sli10})}$ and $\mathscr{D}^{(\text{jit10})}$ are datasets that have been augmented to 10 times the amount of data. $\mathscr{D}^{(\text{sli2}\times\text{jit2})}$ and $\mathscr{D}^{(\text{sli10}\times\text{jit10})}$ are augmented to 4 and 100 times the amount of data by both slicing and jittering, respectively. $\mathscr{D}^{(\text{d-ref})}$ has twice as much data without data augmentation.

For comparisons between datasets, histograms of the ship state variables are presented in Fig. 4, scatter plots is presented in Fig. 5, and the 2D histogram of apparent wind speed and direction are presented in Fig. 6.

These histograms show that both $\mathscr{D}^{(\text{ref})} + \mathscr{D}^{(\text{validation})}$ and $\mathscr{D}^{(\text{d-ref})} + \mathscr{D}^{(\text{validation})}$ are able to cover all the data in $\mathscr{D}^{(\text{test-B})}$, but not all the data in $\mathscr{D}^{(\text{test-R})}$.

For instance, $\mathscr{D}^{(\text{ref})} + \mathscr{D}^{(\text{validation})}$ and $\mathscr{D}^{(\text{d-ref})} + \mathscr{D}^{(\text{validation})}$ does not include sway velocities of above 0.15 m/s existing in $\mathscr{D}^{(\text{test-R})}$. Moreover, $\mathscr{D}^{(\text{test-R})}$ includes the wind state variables of around $U_{\text{A}} = 5.0$ (m/s), $\gamma_{\text{A}} = 300$ (deg.), while $\mathscr{D}^{(\text{ref})}$ does not.

In free-running model tests, it is possible to obtain the dataset that completely covers the test dataset. However, in full-scale trials, it is difficult to do so because of the high costs and its time-consuming nature. In particular, wind disturbances cannot be controlled and large wind speeds rarely occur. In practical use, all possible state variables cannot be included in the training data, and there is a large possibility of encountering state variables that are not included in the training data. Therefore, this study shows the generalization performance for extrapolated state variables not included in the training data.

To demonstrate that the distribution of measured data covers not only the prepared berthing dataset but also a wide range of typical maneuvering behaviors in port operations, a comparison is presented between measured data and the navigation data measured on the full-scale ship during port entry and departure. Miyauchi et al. [48] have conducted a study on the statistical analysis of port navigation and maneuvering of the subject ship used in this study. They recorded data on maneuvering motions of the full-scale ship, and based on this data, presented statistical characteristics of maneuvering motions when entering and leaving port. Consequently, the statistical characteristics of the measured data were compared with the analysis results of Miyauchi et al. Here, since the scale of measured data differed from that of the full-scale ship data, comparisons were made using the similarity rule or non-dimensional values.

Let us focus on the ground speed and drift angle near the moored position. In the literature [48], it is shown that a drift angle is often large when the Euclidean distance from the moored position L_{D} is less than $2.0L_{\text{pp}}$. The histogram of speed over ground $U = \sqrt{u^2 + v_{\text{m}}^2}$ in that condition is shown in Figure 5 of [48], and the same figure are shown in Fig. 7a. Here, β denotes the drift angle. From Fig. 7a, we see that a large drift angle is taken when U is less than 1.5 knots in the berthing and unberthing maneuver.

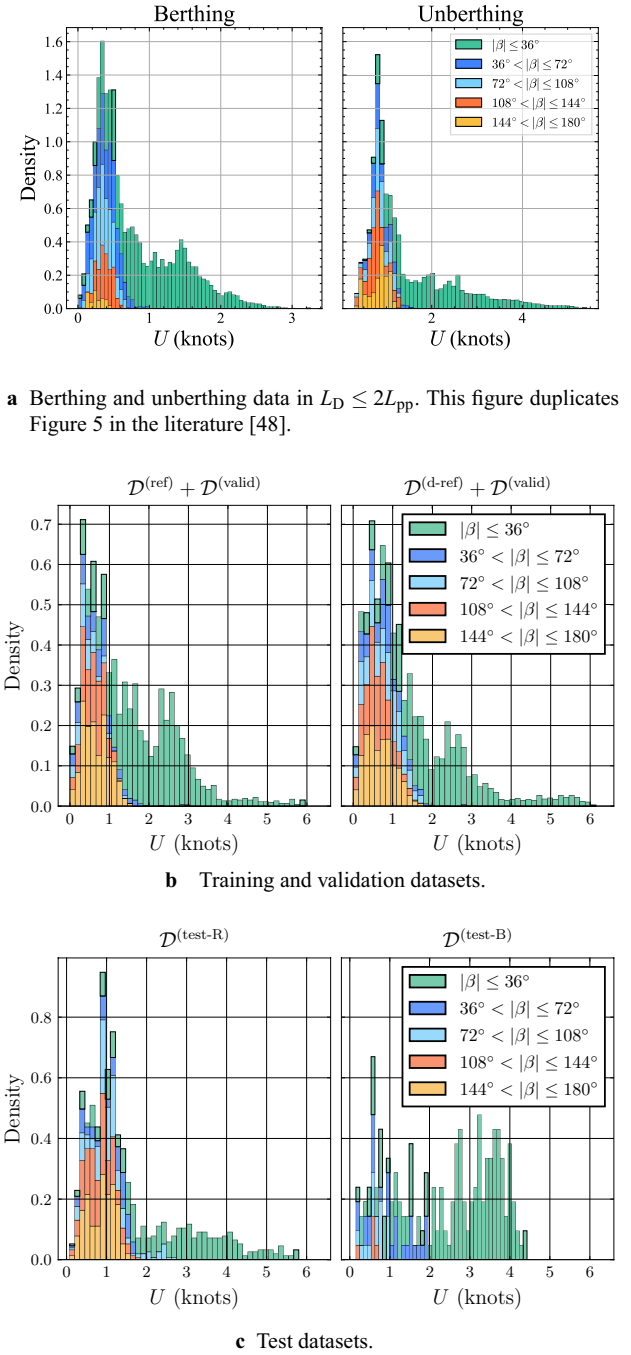

a Berthing and unberthing data in $L_{\text{D}} \leq 2L_{\text{pp}}$. This figure duplicates Figure 5 in the literature [48].

b Training and validation datasets.

c Test datasets.

Fig. 7 Histograms of $|\beta|$ for U. Histograms are normalized so that the sum of their areas equals 1 in each figure

The same histogram using prepared datasets is shown in Figs. 7b and 7. This figure shows that random maneuvering tests measured low-speed maneuvering data and that when U was less than 1.5 knots, maneuvering motions with large drift angles were measured.

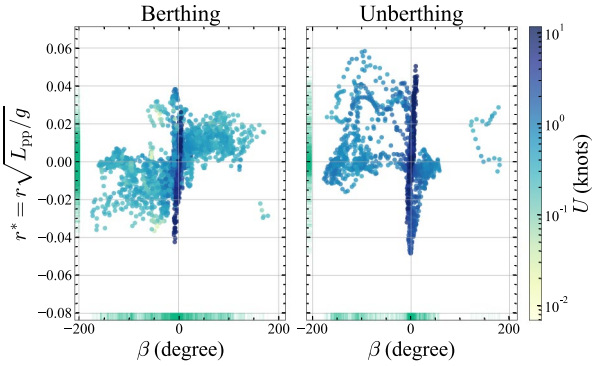

a Berthing and unberthing data. This figure duplicates Figure 6 in the literature [48].

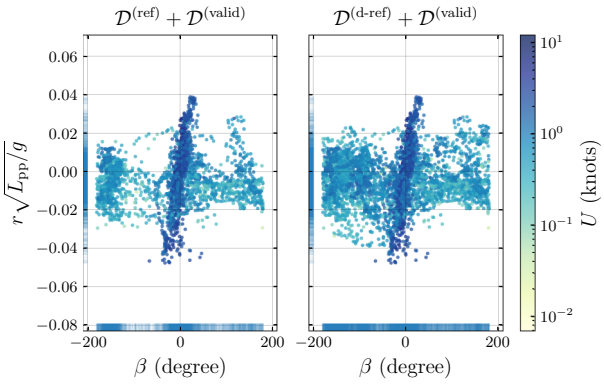

b Training and validation datasets.

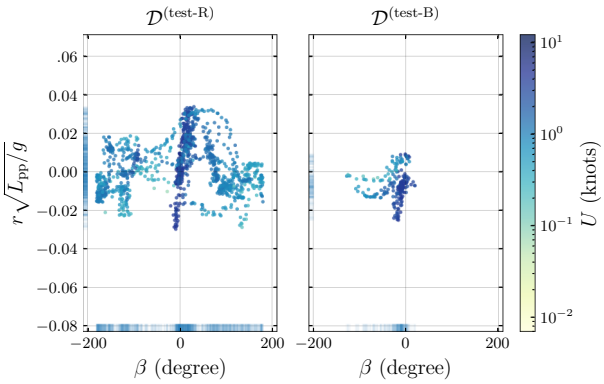

c Test datasets.

Fig. 8 Scatter plots of β and non-dimensionalized yaw velocity $r^* = r\sqrt{L_{pp}/g}$

We also focus on the relationship between β and r. In the literature [48], r is non-dimensionalized by Kose's method [4] and its non-dimensional value is defined as $r^* = r\sqrt{L_{pp}/g}$. The scatter plot of r^* and β is shown in Figure 6 of [48], and the same figure is shown in Fig. 8a. From Fig. 8a, it can be seen that when the ship's speed is sufficiently large, there is a strong positive correlation data measured between r and β for a small range of drift angles. This feature is also seen in the zigzag and turning data [1]. On the other hand, a wide range of drift angles are measured in low-speed conditions, such as less than 1 knot. In particular, in the berthing data, the dimensionless yaw velocity r^* is distributed in the range of −0.02 to 0.02, and a positive correlation with a gradual slope is found between r and β.

Furthermore, the scatter plot of r^* and β using prepared datasets is shown in Fig. 8b, c. Figure 8b, c show random maneuvering test data also had a strong positive correlation between r and β when the ship's speed is sufficiently large. In low-speed conditions, maneuvering motion data are measured for a wide range of drift angles. In particular, r^* of $\mathcal{D}^{(d\text{-}ref)}$, which has a large amount of data, is widely distributed at any drift angle.

Therefore, the random maneuvering test measured not only moderate-speed maneuvering motions with a strong correlation between r and β but also low-speed maneuvering motions with a wide range of drift angles. The distribution of the measured data covered most of the distribution of full-scale data of port maneuvering motions.

Table 5 Hyperparameters in training

Learning rate	1.0×10^{-4}
λ of Eq. 11	1.0×10^{-2}
$\boldsymbol{w}$ of Eq. 10	$(0, 100, 0, 100, 0, 10)^{\mathsf{T}}$
$\Sigma_{\boldsymbol{x}}$	$\mathrm{Diag}(0.0, 0.01^2, 0.0,$ $0.0, 0.01^2, 0.0, 0.1^2)$

4.2 Optimization results

In this subsection, the optimization results are presented.

The hyperparameters used in training are presented in Table 5. Note that the 1, 3, and 5 components of $\boldsymbol{w}$ are set to zero, to ignore the errors of the position and heading angle. The covariance matrix $\Sigma_{\boldsymbol{x}}$ is determined so that noise is added only to the velocity and angular velocity.

The optimization was conducted 10 times for each dataset presented in Table 4 by changing the random number. The optimal parameter was computed for each training dataset and each random number. The exponential moving average values of the evaluation function using the validation dataset at each epoch are presented in Fig. 9. Note that the exponential moving average values were calculated as follows:

$$\hat{\mathscr{L}}_i = \begin{cases} \alpha \mathscr{L}_i + (1-\alpha)\hat{\mathscr{L}}_{i-1} & (i \neq 0) \\ \mathscr{L}_0 & (i = 0) \end{cases}, \tag{24}$$

where $\alpha = 0.1$, $\mathscr{L}_i$ means the evaluation function values of the i-th epoch, and $\hat{\mathscr{L}}_i$ means the exponential moving average ones. The training was terminated when the number of epochs exceeded 10, 000 and the value of the evaluation function values for the validation dataset satisfied the following inequality:

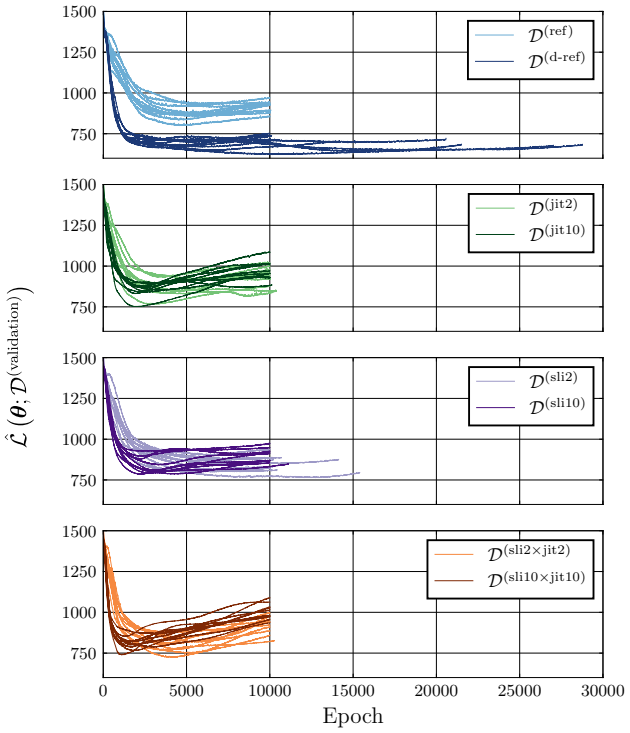

Fig. 9 Exponential moving average values of the evaluation function in the validation dataset. The legend implies the used training dataset. Ten training results with different random numbers for each dataset are presented

$$\mathscr{L}(\boldsymbol{\theta}) > 0.1 \times \left(\mathscr{L}(\boldsymbol{\theta}_{\mathrm{init}}) - \mathscr{L}(\boldsymbol{\theta}_{\mathrm{min}})\right) + \mathscr{L}(\boldsymbol{\theta}_{\mathrm{min}}) \quad . \tag{25}$$

Here, $\boldsymbol{\theta}_{\mathrm{init}}$ denotes the initial parameter and $\boldsymbol{\theta}_{\mathrm{min}}$ denotes the parameter with the smallest values during training. In Eq. 25, the used dataset $\mathscr{D}^{(\mathrm{validation})}$ is omitted for simplicity.

Figure 9 shows that the training was terminated by satisfying Eq. 25 in all cases. These results indicate that overfitting to the training dataset occurred.

Therefore, in this study, the optimal parameters are the parameters with the smallest values of the evaluation function for the validation dataset to avoid overfitting and are denoted as $\boldsymbol{\theta}_{\mathrm{opt}}$.

4.3 Prediction results

The prediction results of dynamic models with optimal parameters $\boldsymbol{\theta}_{\mathrm{opt}}$ are presented here.

The prediction error of dynamic models on the test data was computed, and the evaluation function $\mathscr{L}(\boldsymbol{\theta}_{\mathrm{opt}};\mathscr{D}^{(\mathrm{test\text{-}R})})$ was calculated. The obtained values of the evaluation function and its average value for random numbers are shown in Fig. 10. To show the details of the prediction result, the time series of control inputs and relative wind speed and direction in the test dataset are presented in Figs. 11, and 12 show the

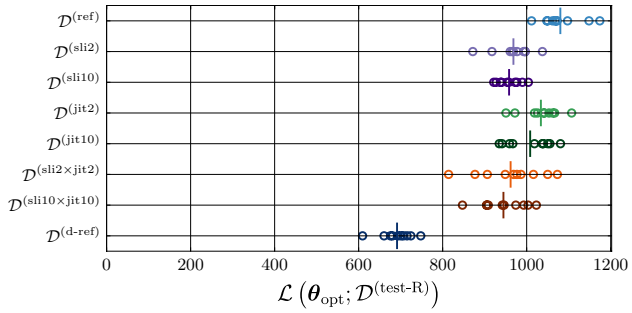

Fig. 10 Evaluation function values for random maneuver $\mathscr{D}^{(\mathrm{test\text{-}R})}$. Vertical bars represent mean values

time series of the ship state variables $\boldsymbol{x}$, the predicted ship state variables $\boldsymbol{x}^{\mathrm{sim}}$, and the temporary errors $d(\boldsymbol{x}^{\mathrm{sim}},\boldsymbol{x})$.

In maneuvering simulation, the number of time steps is $I = 100$. In other words, the predicted ship state variables $\boldsymbol{x}^{\mathrm{sim}}$ were initialized with the measured one $\boldsymbol{x}$ every 100 time steps (100 s).

First, we focus on the dataset augmented by slicing. Figure 10 shows that the mean values of the evaluation function for $\mathscr{D}^{(\mathrm{sli2})}$ and $\mathscr{D}^{(\mathrm{sli10})}$ are smaller than that for $\mathscr{D}^{(\mathrm{ref})}$. This indicates that slicing improves the generalization performance regarding $\mathscr{D}^{(\mathrm{test})}$. However, since there is no significant difference between $\mathscr{D}^{(\mathrm{sli10})}$ and $\mathscr{D}^{(\mathrm{sli2})}$, increasing the amount of data augmented by slicing does not necessarily improve generalization performance.

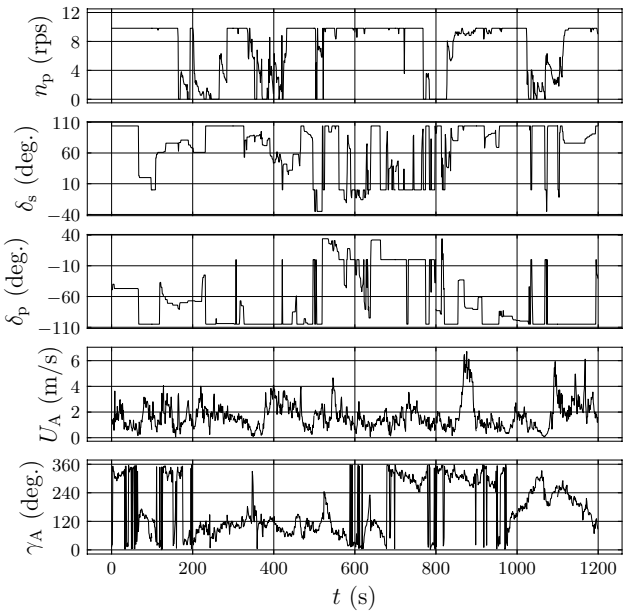

Fig. 11 Time series data of control inputs $\boldsymbol{u}$ and apparent wind velocity and direction $\boldsymbol{\omega}$ in random maneuver $\mathscr{D}^{(\mathrm{test\text{-}R})}$

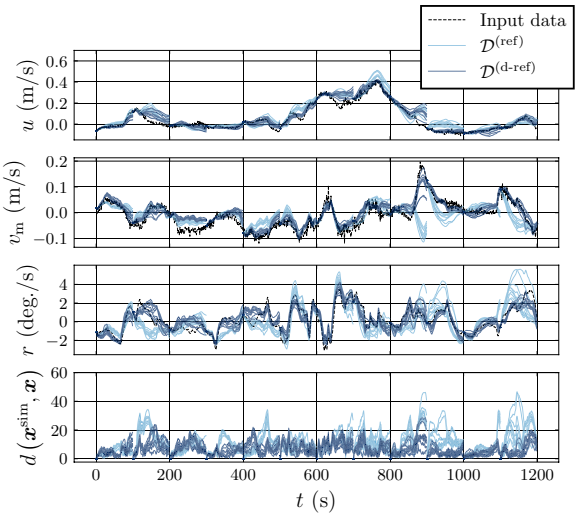

a Results using dynamic models with optimal parameters trained by $\mathscr{D}^{(\mathrm{ref})}$ and $\mathscr{D}^{(\mathrm{d\text{-}ref})}$.

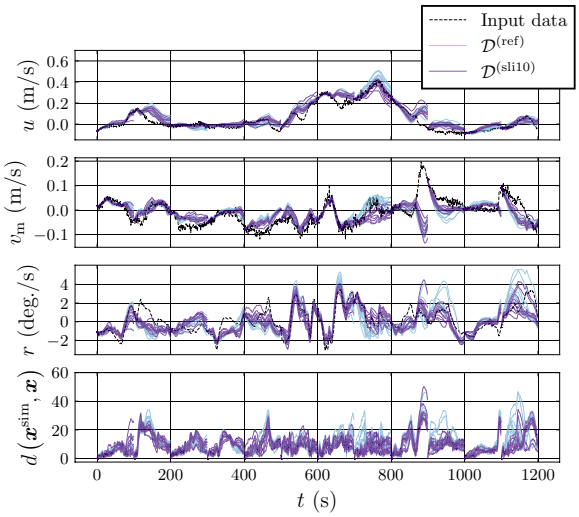

b Results using dynamic models with optimal parameters trained by $\mathscr{D}^{(\mathrm{ref})}$ and $\mathscr{D}^{(\mathrm{sli10})}$.

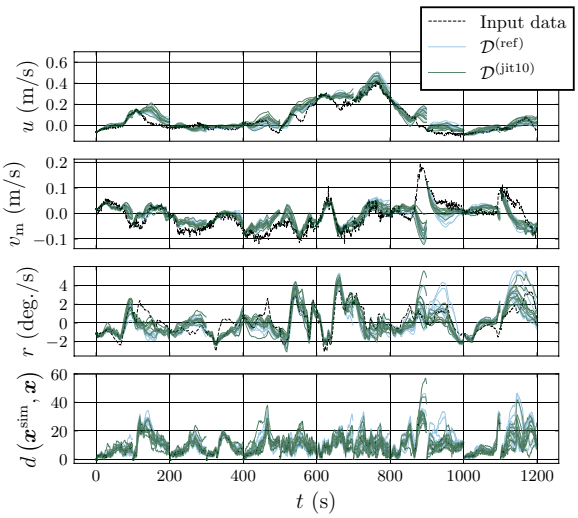

c Results using dynamic models with optimal parameters trained by $\mathscr{D}^{(\mathrm{ref})}$ and $\mathscr{D}^{(\mathrm{jit10})}$.

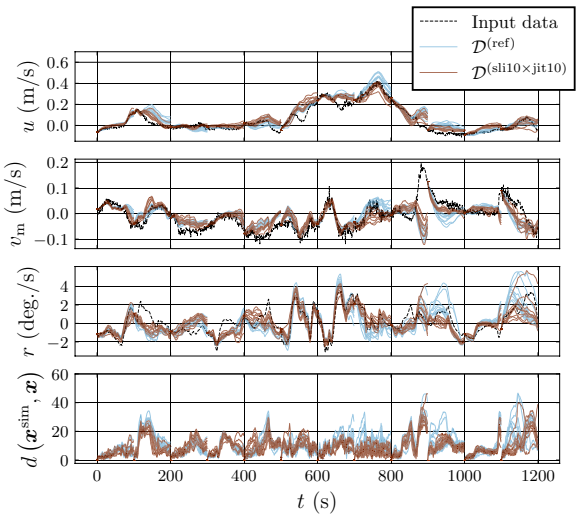

d Results using dynamic models with optimal parameters trained by $\mathscr{D}^{(\mathrm{ref})}$ and $\mathscr{D}^{(\mathrm{sli10\times jit10})}$

Fig. 12 Prediction result of ship state variables $\boldsymbol{\nu}$ and error $d(\boldsymbol{x}^{\mathrm{sim}}, \boldsymbol{x})$ in random maneuver $\mathscr{D}^{(\mathrm{test\text{-}R})}$

Next, we compare the results of $\mathscr{D}^{(\mathrm{ref})}$ and the dataset augmented by jittering, $\mathscr{D}^{(\mathrm{jit2})}$ or $\mathscr{D}^{(\mathrm{jit10})}$. Although the mean values of the evaluation function for $\mathscr{D}^{(\mathrm{jit2})}$ are only slightly smaller than those of $\mathscr{D}^{(\mathrm{ref})}$, that for $\mathscr{D}^{(\mathrm{jit10})}$ are even smaller. Thus, Jittering is also an augmentation method that improves the generalization performance regarding $\mathscr{D}^{(\mathrm{test})}$.

Then, Fig. 10 shows that the mean values of the evaluation function for the dataset augmented by simultaneous slicing and jittering, $\mathscr{D}^{(\mathrm{sli2\times jit2})}$ and $\mathscr{D}^{(\mathrm{sli10\times jit10})}$ are smaller than that for $\mathscr{D}^{(\mathrm{ref})}$. These results indicate that slicing and jittering can be used in combination.

However, the evaluation function values of $\mathscr{D}^{(\mathrm{d\text{-}ref})}$ are smaller than that of any augmented dataset. Even though $\mathscr{D}^{(\mathrm{sli10})}$ and $\mathscr{D}^{(\mathrm{jit10})}$ have more data than $\mathscr{D}^{(\mathrm{d\text{-}ref})}$, the prediction error trained by $\mathscr{D}^{(\mathrm{sli10})}$ and $\mathscr{D}^{(\mathrm{jit10})}$ is not smaller than that by $\mathscr{D}^{(\mathrm{d\text{-}ref})}$.

One reason for this is the difference in prediction errors occurring from 850 to 900 s. Figure 14a shows that $\mathscr{D}^{(\mathrm{d\text{-}ref})}$ reduce that prediction error, while Fig. 14b–d shows that the augmented datasets cannot. Figure 11 shows that the relatively strong apparent wind, which is around $U_\mathrm{A} = 5.0\,(\mathrm{m/s}), \gamma_\mathrm{A} = 300\,(\mathrm{deg.})$, occurred from 850 to 900 s.

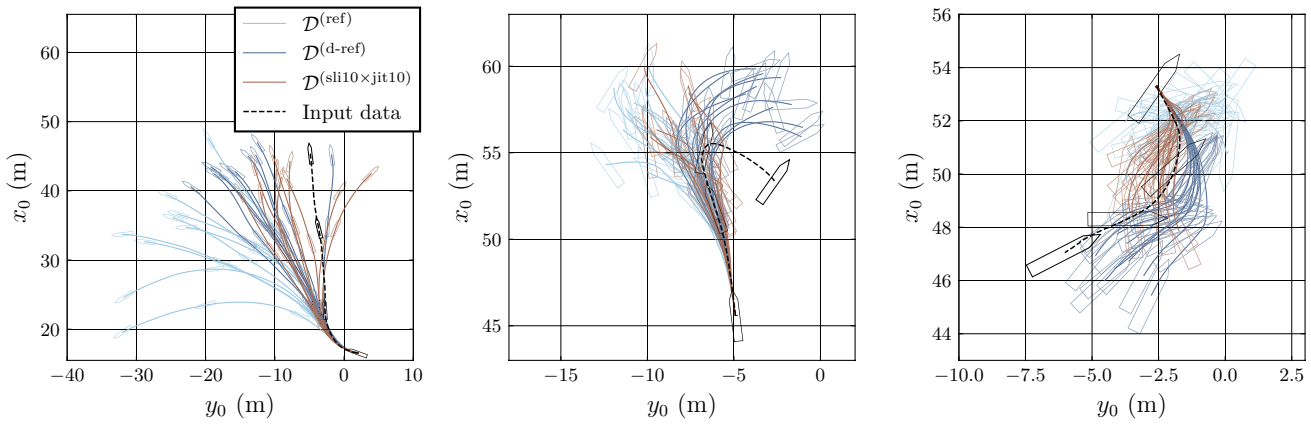

a Trajectories from 700 to 800 s **b** Trajectories from 800 to 900 s **c** Trajectories from 900 to 1000 s

Fig. 13 Predicted results of trajectories in random maneuver $\mathcal{D}^{(\mathrm{test\text{-}R})}$. Dynamic models with optimal parameters trained by $\mathcal{D}^{(\mathrm{ref})}$, $\mathcal{D}^{(\mathrm{d\text{-}ref})}$ and $\mathcal{D}^{(\mathrm{sli10\times jit10})}$ are used

Figure 6 shows that there is a large difference between $\mathcal{D}^{(\mathrm{ref})}$ and $\mathcal{D}^{(\mathrm{d\text{-}ref})}$ in the amount of data around $\gamma_{\mathrm{A}} = 300$ (deg.), $U_{\mathrm{A}} = 5.0$ (m/s). Note that slicing and jittering cannot synthesize data that are not close to any data in the original dataset. Therefore, the data augmentation methods could not reduce the prediction errors occurring from 850 to 900 s. In addition, the prediction errors occurring from 1100 to 1200 s are likely caused by the same reason. As a result, the evaluation function values of $\mathcal{D}^{(\mathrm{d\text{-}ref})}$ becomes the smallest in any other training dataset.

Trajectories of $\boldsymbol{\eta}$ are presented in Fig. 13. Here, Fig. 13 shows the maneuvering simulation results from 700 to 1000 s. In Fig. 13a, surge velocity is relatively large, and trajectories tend to deviate due to accumulated errors in yaw velocity. In particular, the deviation of $\mathcal{D}^{(\mathrm{ref})}$ is large, while that of $\mathcal{D}^{(\mathrm{d\text{-}ref})}$ and $\mathcal{D}^{(\mathrm{sli10\times jit10})}$ is relatively small. In Fig. 13b, the surge velocity shows a significant decrease, and the relatively strong apparent wind occurred from 850 s. The trajectory of $\mathcal{D}^{(\mathrm{d\text{-}ref})}$ shows relatively good agreement with the experimental data, while the trajectories of $\mathcal{D}^{(\mathrm{ref})}$ and $\mathcal{D}^{(\mathrm{sli10\times jit10})}$ deviate in the opposite side from the experimental data after 850 s. Figure 13c starts with the motion maneuvering in the sway direction with surge velocity near zero. In this case, $\mathcal{D}^{(\mathrm{d\text{-}ref})}$ shows the best agreement with experimental results, and the trajectory of $\mathcal{D}^{(\mathrm{sli10\times jit10})}$ is closer to experimental results than that of $\mathcal{D}^{(\mathrm{ref})}$. Therefore, it is evident that the trajectory of $\mathcal{D}^{(\mathrm{d\text{-}ref})}$ demonstrates relatively good agreement with the experimental results. Furthermore, there are cases where $\mathcal{D}^{(\mathrm{sli10\times jit10})}$ exhibits an even better alignment compared to $\mathcal{D}^{(\mathrm{ref})}$.

Finally, to demonstrate the performance of the trained model for berthing maneuver, the prediction results of $\mathcal{D}^{(\mathrm{test\text{-}B})}$ are presented in Fig. 14. Here, the optimal parameter with the smallest value of $\mathscr{L}(\boldsymbol{\theta}_{\mathrm{opt}};\mathcal{D}^{(\mathrm{test\text{-}R})})$ was used. In Trajectory No. 7, models trained with any of the training datasets predict the surge velocity u and sway velocity v_{m} with high accuracy. However, the yaw angle velocity r deviates from the measured data around $t = 30$ (s), causing the trajectory to deviate after this point. For Trajectory No. 8, the model trained by $\mathcal{D}^{(\mathrm{ref})}$ predicts the sway velocity v_{m} and yaw angle velocity r accurately, but the surge velocity u gradually deviates from the measured data, resulting in a significant divergence of the trajectory from the measured data. Conversely, models trained by $\mathcal{D}^{(\mathrm{d\text{-}ref})}$ and $\mathcal{D}^{(\mathrm{sli10\times jit10})}$ continue to predict the surge velocity u with high accuracy, resulting in trajectories that closely match the measured data.

5 Discussion

In Sect. 4.3, the results of numerical experiments to identify a dynamic model for the automatic berthing and unberthing controller were presented. In this study, the dynamic model was represented using an NN-based model, and time-series data measured in the random maneuvers were used as datasets. In numerical experiments, slicing or jittering improved the generalization performance of the dynamic model. The simultaneous use of slicing and jittering also improved the same. Therefore, they were effective data augmentation methods when the amount of measured data was limited.

On the other hand, slicing and jittering cannot synthesize data that is not close to any data in the original dataset and could not improve the generalization performance of the dynamic model within the extrapolation region of the original dataset.

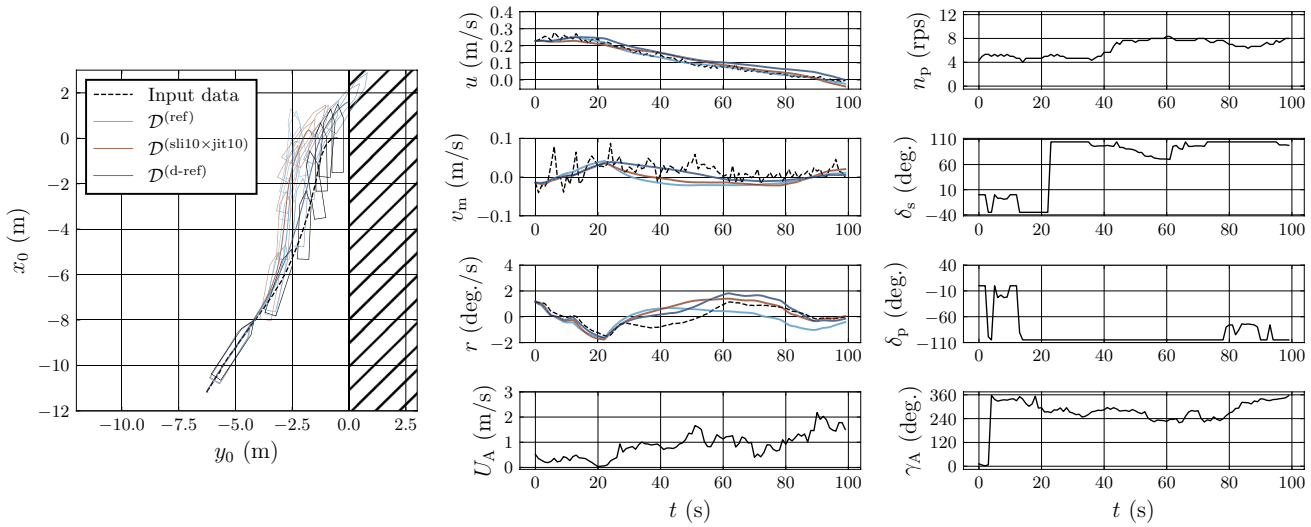

a Trajectory No. 7 of manual berthing maneuver. The diagonal hatch means an imaginary berth.

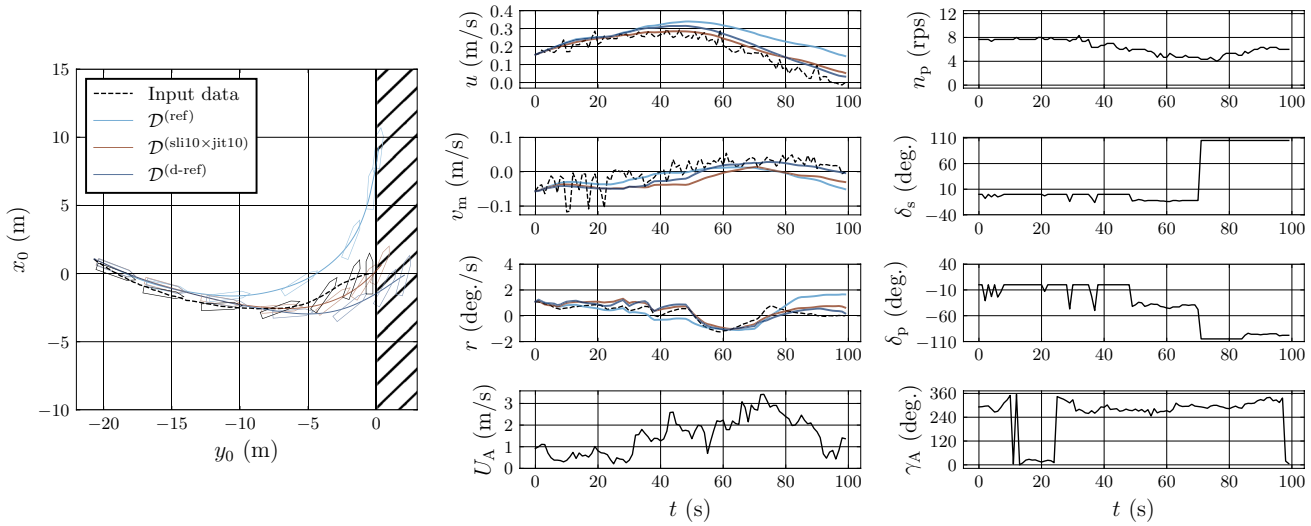

b Trajectory No. 8 of manual berthing maneuver. The diagonal hatch means an imaginary berth.

Fig. 14 Prediction results of manual berthing maneuver with an imaginary berth $\mathscr{D}^{(\mathrm{test\text{-}B})}$ using dynamic models with optimal parameters trained by $\mathscr{D}^{(\mathrm{ref})}$, $\mathscr{D}^{(\mathrm{d\text{-}ref})}$ and $\mathscr{D}^{(\mathrm{sli10\times jit10})}$

For example, strong winds that did not appear in the training data may cause a great deterioration of the generalization performance, and this deterioration cannot be avoided by slicing or jittering. Therefore, when random maneuvering tests or trials are used, it is desirable to measure the data that are widely distributed and have few extrapolation regions.

The dynamic model with optimal parameters was able to estimate the prepared berthing maneuvers with high accuracy. One of the reasons for this is that the distribution of the training data for random maneuvers covers the distribution of the berthing maneuvers, as demonstrated in Fig. 4 and Fig. 6. Therefore, it can be seen that data collection by random maneuvering is one of the effective methods in identification of a dynamic model for harbor maneuvers.

While random maneuvering tests can collect widely distributed maneuvering data, this test lacks reproducibility due to the manual nature of random maneuvers. Thus, it is necessary for future research to focus on data collection methods and explore the incorporation of conventional tests, such as zig-zag, spiral, and turning tests.

It is impractical to observe the desired data with limited measurement time due to uncontrollable wind disturbances. To improve the generalization performance of the extrapolated state, we may need to incorporate physical or hydrodynamic knowledge in addition to the measured data.

These remaining issues are our future works.

6 Conclusion

In this study, data augmentation was introduced to the identification problem to improve the generalization performance of the dynamic model for a berthing and unberthing controller. Slicing and jittering were used as data augmentation methods, and the method for applying these techniques to identification problems of the dynamic model using ANN was demonstrated. The parameters of the dynamic model were identified by minimizing the error between the measured state variables and the state variables simulated by the dynamic model. To validate the effectiveness of the data augmentation methods, numerical experiments were conducted. In numerical experiments, the dynamic model was represented by an NN-based model, and time-series data measured in free-running model tests of the random maneuvers and manual berthing maneuvers with an imaginary berth were used as datasets. The findings of the numerical experiments are summarized as follows:

- Slicing and jittering improved the generalization performance of the dynamic model when the amount of measured data was limited.
- Slicing and jittering did not improve the generalization performance of the dynamic model within the extrapolation region of the original dataset because they cannot synthesize data that is not close to any of the measured data.

Therefore, we confirmed that slicing and jittering were effective data augmentation methods in those numerical experiments.

On the other hand, it was found necessary to collect data that are widely dispersed to reduce extrapolation regions when random maneuvering tests are used to identify a dynamic model for the automatic berthing and unberthing controller.

Acknowledgements This study was supported by a scholarship from the Shipbuilders' Association of Japan (REDAS), and a Grant-in-Aid for Scientific Research from the Japan Society for the Promotion of Science (JSPS KAKENHI Grant #22H01701 and #23KJ1432). The authors would like to express gratitude to Japan Hamworthy & Co., Ltd for the technical discussion, and to Enago (www.enago.jp) for reviewing the English language. The authors would like to thank members of the Ship Intelligentization Subarea, Osaka University, for conducting the model experiment: Hiroaki Koike, Nozomi Amano, Yuta Fueki, and Dimas M. Rachman. Finally, the authors would like to thank the referees for their detailed comments, helpful advice, and suggestions.

Funding Open Access funding provided by Osaka University.

Data availability Due to the nature of the research, participants of this study did not agree for their data to be shared publicly, so we are unable to disclose the supporting data.

Declarations

Conflict of interest The authors declare that they have no Conflict of interest.

References

1. Abkowitz MA (1980) Measurement of hydrodynamic characteristics from ship maneuvering trials by system identification. Trans Soc Naval Arch Marine Eng 88:283–318
2. Ogawa A, Kasai H (1978) On the mathematical model of manoeuvring motion of ships. Int Shipbuild Prog 25:306
3. Yasukawa H, Yoshimura Y (2015) Introduction of MMG standard method for ship maneuvering predictions. J Marine Sci Technol 20(1):37
4. Kose K, Hinata H, Hashizume Y, Futagawa E (1984) On a mathematical model of maneuvering motions of ships in low speeds. J Soc Naval Arch Jpn 1984(155):132
5. Fujino M, Kagemoto H, Ishii Y, Joraku H (1990) Stopping ability of a ship in shallow water. J Soc Naval Arch Jpn 1990(168):117
6. Kobayashi H, Ishibashi A, Shimokawa K, Shimura Y (1994) A study on mathematical model for the maneuvering motions of twin-propeller twin-rudder ship: In reference to the maneuvering motion from ordinary speed range to low speed range. J Jpn Inst Navig 91:263
7. Ishibashi A, Kobayashi H, Ugajin T (1996) A study on ship maneuvering characteristics in shallow water: On the harbor maneuvering at low speed range. J Jpn Inst Navig 95:371
8. Yoshimura Y, Nakao I, Ishibashi A (2009) Unified mathematical model for ocean and harbour manoeuvring. In: Proceedings of MARSIM2009 (International Conference on Marine Simulation and Ship Maneuverability), pp. 116–124
9. Miyauchi Y, Maki A, Akimoto Y, Umeda N (2021) 4-Quadrant Abkotwitz model applicable for complex low-speed maneuver include berthing and unberthing. Conf Proc Jpn Soc Naval Arch Ocean Eng 33:49–58
10. Miyauchi Y, Akimoto Y, Umeda N, Maki A (2023) Development of a mathematical model for harbor-maneuvers to realize modeling automation. arXiv preprint
11. Chislett MS, Strom-Tejsen J (1965) Planar motion mechanism tests and full-scale steering and manoeuvring predictions for a Mariner class vessel. Int Shipbuild Prog 12:201
12. Koyama T, Chyu JH, Motora S, Koyanagi M (1975) On the circular motion test technique (cmt) for the maneuverability model test. J Soc Naval Arch Jpn 1975(138):151
13. Obokata J, Yoshimura Y, Sugita M, Nagashima J (1986) Measurement of added mass of ships with unconventional dimensions. J Kansai Soc Naval Arch Jpn 201:1

14. Motora S (1959) On the measurement of added mass and added moment of inertia for ship motions. J Zosen Kiokai 1959(105):83
15. Fujii H, Tuda T (1961) Experimental researches on rudder performance. J Zosen Kiokai 110:31
16. Inoue S, Hirano M, Kijima K (1981) Hydrodynamic derivatives on ship manoeuvring. Int Shipbuild Prog 28:112
17. Kijima K, Katsuno T, Nakiri Y, Furukawa Y (1990) On the manoeuvring performance of a ship with theparameter of loading condition. J Soc Naval Arch Jpn 1990(168):141
18. Sukas OF, Kinaci OK, Bal S (2019) Theoretical background and application of mansim for ship maneuvering simulations. Ocean Eng 192:106239
19. Fujiwara T, Ueno M, Nimura T (1998) Estimation of wind forces and moments acting on ships. J Soc Naval Arch Jpn 1998(183):77
20. Åström K, Källström C (1976) Identification of ship steering dynamics. Automatica 12(1):9
21. Yoon HK, Rhee KP (2003) Identification of hydrodynamic coefficients in ship maneuvering equations of motion by estimation-before-modeling technique. Ocean Eng 30(18):2379
22. Araki M, Sadat-Hosseini H, Sanada Y, Tanimoto K, Umeda N, Stern F (2012) Estimating maneuvering coefficients using system identification methods with experimental, system-based, and cfd free-running trial data. Ocean Eng 51:63
23. Sutulo S, Guedes SC (2014) An algorithm for offline identification of ship manoeuvring mathematical models from free-running tests. Ocean Eng 79:10
24. Miyauchi Y, Maki A, Umeda N, Rachman DM, Akimoto Y (2022) System parameter exploration of ship maneuvering model for automatic docking/berthing using CMA-ES. J Marine Sci Technol 27(2):1065
25. Wakita K, Maki A, Umeda N, Miyauchi Y, Shimoji T, Rachman DM, Akimoto Y (2022) On neural network identification for low-speed ship maneuvering model. J Marine Sci Technol 27(1):772
26. Källström C, Åström K (1981) Experiences of system identification applied to ship steering. Automatica 17(1):187
27. Moreira L, Guedes SC (2003) Dynamic model of manoeuvrability using recursive neural networks. Ocean Eng 30(13):1669
28. Moreira L, Soares CG (2012) Recursive neural network model of catamaran manoeuvring. Int J Marit Eng 154 (Copyright The University of Buckingham Press 2012)
29. Rajesh G, Bhattacharyya S (2008) System identification for nonlinear maneuvering of large tankers using artificial neural network. Appl Ocean Res 30(4):256
30. Oskin DA, Dyda AA, Markin VE (2013) Neural network identification of marine ship dynamics. IFAC Proc 46(33):191 (**9th IFAC Conference on Control Applications in Marine Systems**)
31. Zhang XG, Zou ZJ (2013) Black-box modeling of ship manoeuvring motion based on feed-forward neural network with chebyshev orthogonal basis function. J Marine Sci Technol 18:42
32. Zhang X, Zou Z (2011) Identification of Abkowitz Model for Ship Manoeuvring Motion Using ε-Support Vector Regression. J Hydrodyn 23(3):353
33. Luo W, Moreira L, Guedes Soares C (2014) Manoeuvring simulation of catamaran by using implicit models based on support vector machines. Ocean Eng 82:150
34. Ariza Ramirez W, Leong ZQ, Nguyen H, Jayasinghe SG (2018) Non-parametric dynamic system identification of ships using multi-output gaussian processes. Ocean Eng 166:26
35. Xue Y, Liu Y, Ji C, Xue G, Huang S (2020) System identification of ship dynamic model based on gaussian process regression with input noise. Ocean Eng 216:107862
36. Cybenko G (1989) Approximation by superpositions of a sigmoidal function. Math Control Signals Syst 2(4):303
37. Hornik K (1991) Approximation capabilities of multilayer feedforward networks. Neural Netw 4(2):251
38. Wen Q, Sun L, Yang F, Song X, Gao J, Wang X, Xu H (2021) Time series data augmentation for deep learning: A survey. In: Zhou ZH (ed) Proceedings of the Thirtieth International Joint Conference on Artificial Intelligence, IJCAI-21. (International Joint Conferences on Artificial Intelligence Organization), pp. 4653–4660, survey Track
39. Iwana BK, Uchida S (2021) An empirical survey of data augmentation for time series classification with neural networks. PLos One 16(7):1
40. Le Guennec A, Malinowski S, Tavenard R (2016) Data augmentation for time series classification using convolutional neural networks. In: ECML/PKDD Workshop on Advanced Analytics and Learning on Temporal Data (Riva Del Garda, Italy)
41. Um TT, Pfister FMJ, Pichler D, Endo S, Lang M, Hirche S, Fietzek U, Kulić D (2017) Data augmentation of wearable sensor data for parkinsons disease monitoring using convolutional neural networks. In: *Proceedings of the 19th ACM International Conference on Multimodal Interaction* (Association for Computing Machinery, New York, NY, USA), ICMI '17, p. 216–220
42. Ismail Fawaz H, Forestier G, Weber J, Idoumghar L, Muller PA (2018) Data augmentation using synthetic data for time series classification with deep residual networks. In: International Workshop on Advanced Analytics and Learning on Temporal Data, ECML PKDD
43. Cui Z, Chen W, Chen Y (2016) Multi-scale convolutional neural networks for time series classification
44. Bishop CM (1995) Training with noise is equivalent to tikhonov regularization. Neural Comput 7(1):108
45. Rashid KM, Louis J (2019) Times-series data augmentation and deep learning for construction equipment activity recognition. Adv Eng Inform 42:100944
46. Wakita K, Miyauchi Y, Akimoto Y, Maki A (2023) Data Augmentation Methods of Parameter Identification for Ship Maneuvering Model. In: Conference proceedings, the Japan Society of Naval Architects and Ocean Engineers, vol. 36, vol. 36 (in Japanese)
47. Kingma DP, Ba J (2015) Adam: a method for stochastic optimization. In: Published as a conference paper at the 3rd International Conference for Learning Representations, San Diego. arxiv:1412.6980
48. Miyauchi Y, Kambara T, Umeda N, Hosogaya K, Maki A (2022) Statistical analysis of port navigation and maneuver of a japanese merchant vessel. In: Conference proceedings, the Japan Society of Naval Architects and Ocean Engineers, vol. 35, vol. 35, pp. 77–87 (in Japanese)